Proceedings of ISFOG 2025
5TH INTERNATIONAL SYMPOSIUM ON
FRONTIERS IN OFFSHORE GEOTECHNICS
Nantes, France | June 9-13 2025

ISBN 978-2-85782-758-0

Simulating pile set-up in a DEM centrifuge chamber

J. Lei
Department of Geotechnical Engineering and Geosciences, Polytechnic University of Catalonia (UPC), Barcelona, Spain

M. Arroyo
Department of Geotechnical Engineering and Geosciences, Polytechnic University of Catalonia (UPC), Barcelona, Spain

M. O. Ciantia
School of Science and Engineering, University of Dundee, Dundee, UK

Università Degli Studi di Milano Bicocca, Milan, IT

jiangtao.lei@upc.edu (corresponding author)

ABSTRACT: Pile set-up, defined as the pile shaft capacity increase with time, is a well-established behavioural feature of displacement piles installed in sand. To date, the mechanisms underlying set-up are poorly understood and, as a consequence, is difficult to reliably incorporate this phenomena into design. Micromechanical investigations have recently shown that pile set-up may be directly related to the time dependent breakage of sand around the pile. Following the idea that fracture propagation has an inherent timescale, a fracture based quartz sand discrete element method (DEM) model, previously validated on creep/stress relaxation experimental results, was implemented into a DEM centrifuge chamber to simulate pile set-up. The particle refinement method was implemented to ensure a manageable number of elements. The model pile was either jacked or driven to the target depth. One month creep period under load was applied to age the system. Pull-out pile tests were simulated for the fresh pile and aged pile conditions. The results show a mobilized shaft capacity increase of over 20% for jacked piles and over 50% for driven piles, within the range reported from field pile tests.
Keywords: DEM; particle crushing; quartz sand; sand creep; crack propagation; centrifuge; pile set-up;

1 INTRODUCTION

Pile set-up refers to the increase in shaft capacity of driven piles in granular soil following installation. This phenomenon has been well-documented in numerous in-situ tests (e.g., Chow et al., 1998; Jardine et al., 2006;). The phenomena has proven difficult to reproduce in the laboratory. While some model tests (e.g., Zhang and Wang, 2015) have also reported pile set-up, there are also frequent instances of no observable set-up (Rimoy et al., 2015). Those model tests have almost always been 1g as centrifuge testing is generally considered unpractical for the long periods involved in set-up.

Set-up of jacked piles has also been studied in the field and in laboratory. It is generally admitted that the shaft capacity gain is less than that of driven piles (Lehane, 2012) and set-up of jacked piles takes place at a lower rate than in driven piles.

The discussion about pile set-up is facilitated by reference to a frictional model usually employed (e.g. Jardine et al. 2006) to describe the shaft resistance of displacement piles τ_f:

$$\tau_f = (\sigma'_{rp} + \Delta\sigma'_{rp}) \tan \delta'_f \quad (1)$$

where σ'_{rp} is the stationary radial stress acting on the pile; $\Delta\sigma'_{rp}$ is mobilised radial stress during pile loading; δ'_f is the interface frictional angle.

Therefore, pile set-up may result from increases in σ'_{rp}, $\Delta\sigma'_{rp}$, and/or δ'_f. A possible explanation for these increases would involve the time-dependent behaviour of sands surrounding the pile, specifically: (i) increased soil stiffness and/or dilatancy due to sand ageing leading to a rise of $\Delta\sigma'_{rp}$. (ii) a combination of creep and stress relaxation, resulting in the stress redistribution that increases σ'_{rp} . An alternative explanation highlights the effects of corrosion or chemical processes at the pile-soil interface.

The time-dependent behavior of sands is primarily attributed to physical changes rather than chemical reactions (Mitchell, 2008). Delayed grain fracture has been identified as a plausible mechanism for the time effects observed in sands (Karimpour and Lade, 2010). The discrete element method (DEM) offers a unique advantage in capturing granular-scale phenomena to represent macroscopic behaviour (Ciantia et al. 2019a). Lei (2024) incorporated grain fracture into a

computationally practical model of grain breakage. This model accurately reproduces creep (Lei et al. 2024) and stress relaxation (Lei et al. 2025b), in quartz sands, along with associated particle breakage. Lei et al (2025a) showed how the same model could be applied to simulate set-up of jacked piles. This work extends that later study by examing set-up effect after simulated pile driving.

2 FONTAINEBLEAU SAND MODEL

For the purpose of completeness, the time-to-fracture model reported by Lei et al. (2024) is introduced here briefly, where the response between contact force and contact overlap is controlled by a three-stage rough contact model (Otsubo et al, 2017), developed from the Hertzian contact model, to capture the effect of roughness on sand grain contact stiffness. The time-independent failure proposed by Ciantia et al. (2019b) is given by:

$$F_n \leq \sigma_{\lim,0}\left(\frac{d}{Sd_0}\right)^{-\frac{3}{m_p}}(1+X_{0,1}var)A_F \quad (2)$$

where F_n is the contact normal force, $\sigma_{\lim,0}$ is the reference particle strength at the reference particle diameter d_0 , S is the particle scaling factor adopted when forming the virtual centrifuge chamber, m_p is the size dependent parameter calibrated through particle single crushing tests. $X_{0,1}$ reprents a random number sampled from the standard normal distibution. *Var* represents particle strength variance and A_F contact area between two particles.

Crack propagation induced granular breakage was defined as time-independent failure. Lei et al. (2024) explained that the crack propagation in a particle can be controlled by a normalised Charles law (1958):

$$v = v_0\left(\frac{\sigma_{max}}{\sigma_{lim}}\right)^n \quad (3)$$

where v_0 is a benchmark velocity (0.1 m/s), σ_{max} is the maximum normal contact stress acting on the particle and $\sigma_{lim} = \sigma_{\lim,0}\left(\frac{d}{d_0}\right)^{-\frac{1}{m_p}}(1+X_{0,1}var)$ represents the value of specific strength in each particle.

Each particle is seeded with an initial crack half-length a_0 sampled from a uniform distribution (Tapias et al. 2015). The crack half-length a propagates in time can be explained in the following Equation:

$$a = a_0 + v\Delta t \quad (4)$$

where Δt is the crack updating timestep and v represents crack propagation velocity.

Once F_n reach its limit value (Equation 2) or the crack half-length a is equal to particle radius, the particle will be replaced by 14 sibling particles in an alignment described in Ciantia et al. (2015).

3 OFF-DEM AGEING

Off-DEM ageing can be described as an alternate procedure between dynamic computation and crack propagation induced sample ageing (Lei et al. 2024). This is a strategy to overcome the overwhelming computation load required to reproduce real ageing times (spanning hours to months) in DEM simulations, in which the timestep required by computational stability of the explicit time-marching algorithm is always well below 10^{-6} s. The simulation begins with a dynamic computation where the model cycles for a while to ensure its equilibrium state. During off-DEM ageing only crack propagation is activated, assuming its velocity is constant and is determined by the maximum normal contact force (Equation 3) at the end of a previous dynamic computation stage. During off-DEM ageing computed crack growth would lead to failure of some particles. Such particles are identified and counted until a predefined failure number (n_{age}) is reached. Another round of DEM dynamic computation is resumed to break those particles.

4 VIRTUAL CENTRIFUGE TEST DESIGN

Table 1 shows the parameters calibrated to represent Fontainebleau sand, a typical quartz sand (Lei et al. 2024). Using those parameters simulated creep tests compared favourably with independent laboratory results in terms of creep strain, strain rates, and grading index evolution. These parameters were also employed for the material filling the 3-D centrifuge chamber in this study. The diameter D_c and height H of the chamber are 30 cm and 15 cm, respectively.

To ensure a manageable number of particles, the particle refinement method (PRM) (McDowell et al. 2012) was employed to form the chamber (Figure 1). This is a method in which different scaling factors are applied in concentric shells, increasing from the centre to the side wall of the chamber. The smallest scaling factor S_c=5 is applied to the chamber core section with has a diameter of 1.3 cm. The scaling factor is then multiplied by 1.5 as we move from one section to the next, to avoid particle migration (McDowell et al. 2012).

Different scaled particles were first generated into each section following the corresponding scaled particle size distribution (PSD) shown in Figure 2.

The initial void ratio was 0.642 and the chamber was then cycled with zero particle friction to attain equilibrium (unbalanced force ratio decreased to 10-5) at a reduced void ratio of 0.542. After that, particle friction was recovered and particle strength properties were assigned to all particles. Crack propagation (time-dependent failure) was only activated at the central section (scale 1) for the purpose of computational efficiency. The centrifuge acceleration (50 g) was then applied and the chamber was cycled again to fulfil the same equilibrium state requirement and a denser state (void ratio of 0.482) was attained. Although not directly comparable because of shape differences, this would correspond to a relative density of 107% in Fontainebleau sand.

Table 1 Model parameters for the centrifuge chamber

Category	Parameter/unit	Value
Particle failure criteria	G/GPa	32
	ν	0.19
	μ	0.275
	m	12
	$\sigma_{lim,0}$/GPa	3.75
	var	0.38
	d_c/d_{50}	0.55
	d_{max}/mm	0.27
	d_{min}/mm	0.01
Contact roughness	S_q/μm	0.6
	n_1	0.05
	n_2	5
Crack Propagation	v_0	0.1
	n	60

Note: G=shear modulus; ν= Poisson's ratios; μ= interparticle friction coefficient; dc= particle comminution limit; d_{50}=50% pass particle size; d_{max}, d_{min}=maximum, minimum particle diameter; S_q=particle surface roughness; n_1, n_2= roughness parameters

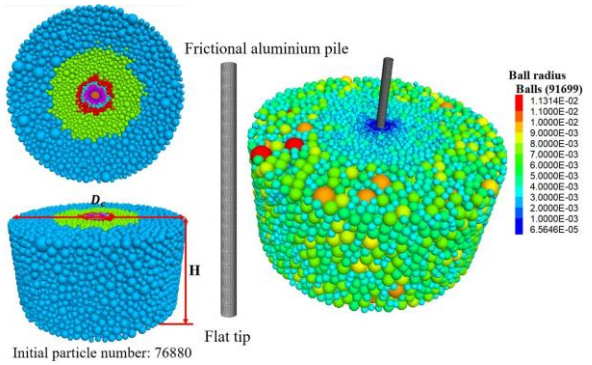

Figure 1. DEM virtual centrifuge chamber and the model pile

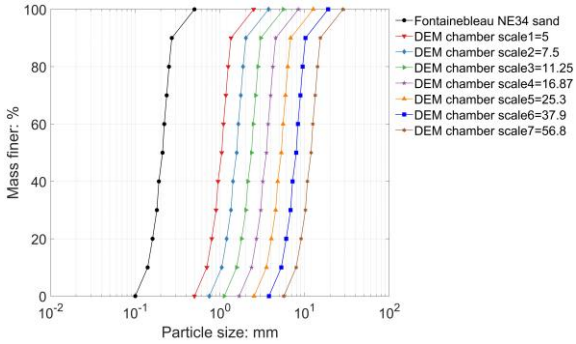

Figure 2. Granular size distribution of Fontainebleau sand with different scaling factors employed in the centrifuge.

A flat tip model pile was formed with a bundle of rigid walls. The model pile diameter d_{pile} was 1 cm resulting in a chamber to pile ratio (D_c/d_{pile}) of 30, large enough to avoid boundary effects (Bolton et al. 1999). The pile to particle diameter ratio (d_{pile}/d_{50}) is 9.5 in this study, larger than those employed in previous DEM studies of pile penetration. The material parameters of the pile were selected as those of aluminium, with shear modulus G of 26 GPa, Poisson's ratio v of 0.33, and frictional coefficient of 0.275.

A representative cubic volumetric element (REV) of side 1.68 cm with the scaling factor of 5 (central scaling) was formed to check whether the real mechanical behaviour of Fontainebleau sand could be reproduced. The oedometer test stopped when the vertical stress reached around 20 MPa, exceeding the maximum penetration resistance recorded during jacked pile installation (next section). Figure 3 compares the result of this test with those of scale 1 DEM model and the equivalent laboratory test results. It is apparent that the void ratio-vertical stress response is similar.

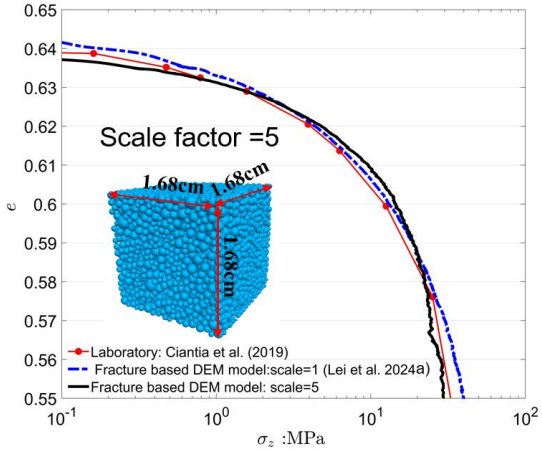

Figure 3. Oedometer curve verification against laboratory results reported by Ciantia et al. (2019b)

5 PILE INSTALLATION AND TESTING

5.1 Pile jacking scheme

The pile was jacked to depth of 60 mm (Prototype 3 m) before carrying out pile creep and tension tests. To ensure the quasi-static condition, the inertial number I can be calculated as:

$$I = \dot{\gamma} S_c d_{50} \sqrt{\rho_p / P} \quad (5)$$

where $\dot{\gamma}$ is the shear strain rate; S_c represents the central scaling factor, d_{50} represents the median grain size, ρ_p represents particle density and P pressure at the chamber bottom.

The ultimate jacking velocity of the pile can be calculated as a function of shearing rate $\dot{\gamma}$ and L_p, the width of plastic zone around pile tip:

$$V_{pie} = \dot{\gamma} L_p \quad (6)$$

The jacked velocity employed was 1.5 m/s, smaller than the critical velocity (1.98 *m/s*) with I of 0.01.

5.2 Pile driving scheme

The impact model reported by Fairhurst (1961) was implemented here to simulate pile driving. Figure 4 shows the scheme of single impact time history. The model has been successfully implemented to simulated standard penetration tests previously (Zhang et al. 2019).

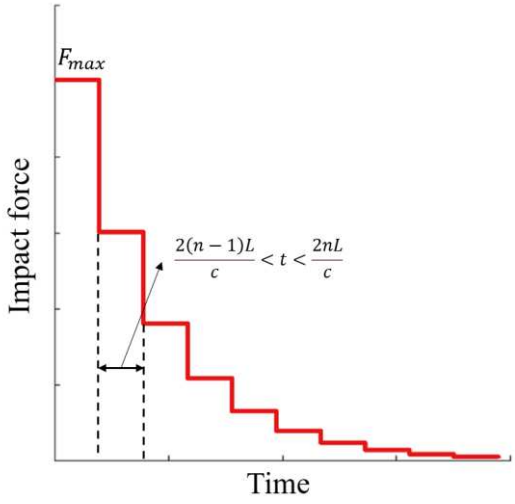

Figure 4. Fairhurst (1961) single impact model

In their model, the maximum driven force is controlled by the following equation:

$$F_{drmax} = \frac{\eta_d a \sqrt{2*50ghE\rho_r}}{1+\left(\frac{a}{A_h}\right)} \quad (7)$$

where η_d represents a dynamic efficiency ratio (set as 1 for default), a and A_h represent the cross-area of the pile and hammer, respectively. $50g$ represents the centrifuge acceleration; h represents the hammer falling height; E elastic modulus of aluminum model pile; ρ_r density of aluminum pile.

The corresponding driving force F_{dr} for the n^{th} (n>1) impact is:

$$F_{drv} = F_{drmax}\left(\frac{1-r}{1+r}\right)^{n-1} \text{ for } \frac{2(n-1)L}{c} < t < \frac{2nL}{c} \quad (8)$$

where r the hammer rod impedance ratio, is given by $\frac{a}{A_h}$. L the hammer length, t the time duration of single impact wave; The wave propagation velocity c is calculated as $\sqrt{E/\rho_r}$; the single driven time $t_{max}=2l/c$, and l is the pile length.

Table 2 shows the parameters adopted in the simulated driving system. The hammer drop height was designed as 49 mm, similar to the value selected by Zhang and Wang (2014) in laboratory driven pile chamber tests. The cross-section area of the hammer is four times that of model pile. F_{drmax} is calculated as 6 kN. The pile was driven to the target penetration depth of 60 mm (prototype 3 m), during which the chamber remains dynamic equilibrium state.

Table 2.Parameters selected for the pile penetration scheme

ρ_r (kg/m^3)	2700
E(GPa)	70
c (m/s)	5092
m_h (kg)	0.96
h (m)	0.049
g (m/s^2)	50g
a (m^2)	7.85e-5
A_h (m^2)	3.14e-4
r (-)	0.25
L (m)	0.05
l (m)	0.12
t_{max}(ms)	0.047
F_{drmax} (kN)	6

5.3 Pile creep

During pile advance to the target depth (60 mm), the total penetration force F was recorded. For the jacked pile, F the penetration force at this target depth was 1.2 kN (at model scale). The driven pile static capacity was evaluated after installation through a separate unload-reload test to 0.9 kN.

This difference indicates a significant loosening of the model during driven installation in the DEM centrifuge. Comparative studies of pile installation effects on a physical centrifuge noted larger densification of loose soils during driving than jacking (Heins et al. 2020), but similar comparisons for initially dense soils are lacking.

After installation to the target depth the piles were unloaded and reloaded statically to 90% of the static capacity. One-month pile creep tests were then performed maintaining this load constant.

6 PILE SET-UP RESULTS

Pile tension load tests at a constant pull-out rate of 0.1 m/s out were conducted before and after a one-month creep period.

6.1 Jacked pile set-up

Figure 5 shows the tension load test results for the jacked pile. It is apparent that the mobilised shaft resistance of jacked pile increased after one month pile creep.

The simulated normalised ultimate shaft resistance τ/τ_n is plotted in Figure 6, together with some in-situ jacked pile set-up results. The ultimate shaft resistance τ was estimated when the first inflection of the tension load curve appeared (Figure 5). τ_0 represents the shaft resistance of the pile before creep. The simulated results are close the in-situ test resuts reported by Lehane (1992) and Chow (1997), although they seem smaller than the results reported at ESP test site (Lim and Lehane, 2015).

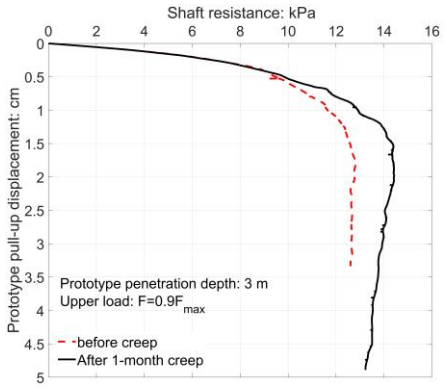

Figure 5. The jacked pile pull-out test results before and after one-month creep

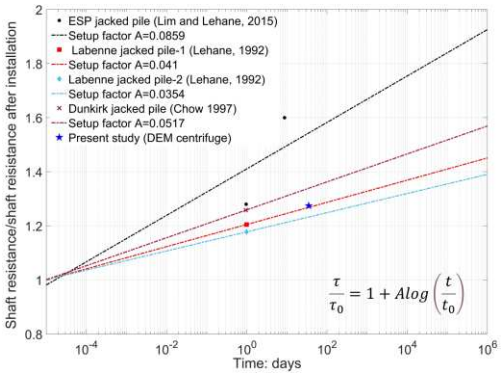

Figure 6. Comparison of jacked pile set-up simulations with in-situ jacked pile set-up results

6.2 Driven pile set-up

Figure 7 shows tension load test results for a driven pile. Although the driven pile has a lower value of shaft capacity than the jacked pile, a larger increase in shaft capacity is observed in the driven pile after one-month of creep. The computed normalised ultimate shaft resistance τ/τ_n is compared with field set-up data in Figure 8. Again the simulation results agree well with field data, both aligned with the intact ageing curve (IAC) proposed by Jardine et al. (2006).

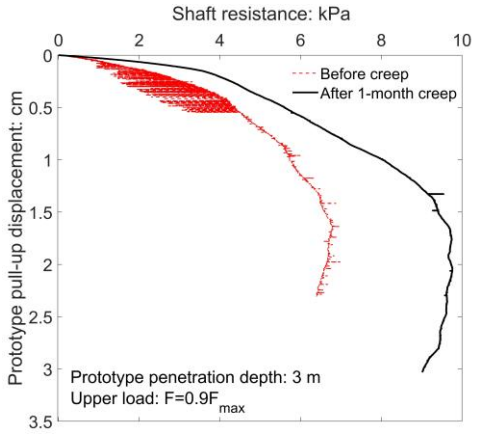

Figure 7 Driven pile pull-out test results before and after one-month creep

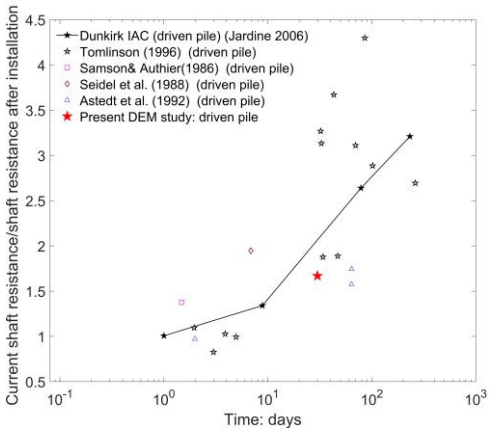

Figure 8. Comparison of driven pile set-up simulations and field data from Jardine et al (2006)

7 CONCLUSIONS

The fracture-based DEM model proposed by Lei et al. (2024, 2025b) was implemented into a virtual centrifuge chamber to study pile set-up. After one-month pile creep shaft capacity increased in jacked and driven pile by 20% and 50%, respectively. This study demonstrates how delayed grain crushing may contribute to a large-scale phenomenon: pile set-up.

More generally this work also shows how DEM might be a valuable tool to address current limitations in experimental pile set-up studies. Validated models such as this enable the identification and analysis of influential factors affecting set-up in field and laboratory tests, providing a firmer basis for design procedures incorporating set-up .

AUTHOR CONTRIBUTION STATEMENT

J. Lei: Data curation, Formal Analysis, Writing- Original draft. **M. Arroyo**: Conceptualization, Funding acquisition, Methodology, Supervision, Writing- Review and Editing. **M**. **Ciantia**: Methodology, Supervision, Writing- Review and Editing.

ACKNOWLEDGEMENTS

Spanish Research Agency support (AEI) through research project PID2020-119598RB-I00 is acknowledged.

REFERENCES

Arroyo, M., Butlanska, J., Gens, A., Calvetti, F., Jamiolkowski, M., (2011). Cone penetration tests in a virtual calibration chamber. *Géotechnique* 61 (6), 525–531.

Bolton, M. D., et al. (1999). Centrifuge cone penetration tests in sand. *Geotechnique*, 49(4), 543–552.

Charles, R. J. (1958). Static fatigue of glass. *J. Appl. Phys.* 29, No. 11, 1549–1560.

Chow, F. C., Jardine, R. J., Brucy, F., & Nauroy, J. F. (1998). Effects of time on capacity of pipe piles in dense marine sand. *J. Geotech. Geoenviron*, *124*(3), 254-264.

Ciantia, M. O., Arroyo, M., Calvetti, F. & Gens, A. (2015). An approach to enhance efficiency of dem modelling of soils with crushable grains. *Géotechnique* 65, No. 2, 91–110.

Ciantia, M., O'Sullivan, C., & Jardine, R. J. (2019a). Pile penetration in crushable soils: Insights from micromechanical modelling. In *Proceedings of the XVII ECSMGE-2019*.

Ciantia, M. O., Arroyo, M., O'Sullivan, C., Gens, A. & Liu, T. (2019b). Grading evolution and critical state in a discrete numerical model of Fontainebleau sand. *Géotechnique* 69, No. 1, 1–15

Fairhurst, C., 1961. Wave mechanics of percussive drilling. Mine and Quarry Engineering 27 (3), 122–130.

Heins, E., Bienen, B., Randolph, M. F., & Grabe, J. (2020). Effect of installation method on static and dynamic load test response for piles in sand. International journal of physical modelling in geotechnics, 20(1), 1-23.

Jardine, R. J., Standing, J. R., & Chow, F. C. (2006). Some observations of the effects of time on the capacity of piles driven in sand. *Géotechnique*, *56*(4), 227-244.

Karimpour, H., & Lade, P. V. (2010). Time effects relate to crushing in sand. *J. Geotech. Geoenviron*, 136(9), 1209-1219.

Lehane, B.M. 1992. Experimental investigation of pile behaviour using instrumented field piles. *Ph.D. thesis, University of London* (Imperial College), London.

Lehane, B. M., Schneider, J. A., Lim, J. K., & Mortara, G. (2012). Shaft friction from instrumented displacement piles in an uncemented calcareous sand. *J. Geotech. Geoenviron*, 138(11), 1357-1368

Lei, J., Arroyo, M., Ciantia, M. O., & Zhang, N. (2024). A fracture-based discrete model for simulating creep in quartz sands. *Géotechnique*, 1-15.

Lei et al (2025a). Simulation of grain fracture induced pile creep and set-up in sands *J. Geotech. Geoenviron* 10.1061/JGGEFK/GTENG-14279 (Accepted)

Lei, J., Arroyo, M., Ciantia, M. O., & Zhang, N. (2025b). A breakage-based discrete element study of stress relaxation in quartz sands, *Acta Geotechnica, doi /10.1007/s11440-025-02592-0*

Lim, J. K., & Lehane, B. (2015). Time effects on shaft capacity of jacked piles in sand. *Canadian Geotechnical Journal*, *52*(11), 1830-1838.

McDowell, G. R., Falagush, O., & Yu, H. S. (2012). A particle refinement method for simulating DEM of cone penetration testing in granular materials. *Géotechnique Letters*, *2*(3), 141-147.

Mitchell, J. K. (2008). Aging of sand – a continuing enigma? Proceedings of the 6th international conference on case histories in geotechnical engineering, Arlington, VA, USA, pp. 1–21. Rolla, MO, USA

Otsubo, M., O'Sullivan, C., Hanley, K. J. & Sim, W. W. (2017). The influence of particle surface roughness on elastic stiffness and dynamic response. *Géotechnique* 67, No. 5, 452–459.

Rimoy, S., Silva, M., Jardine, R., Yang, Z. X., Zhu, B. T., & Tsuha, C. D. H. (2015). Field and model investigations into the influence of age on axial capacity of displacement piles in silica sands. *Géotechnique*, *65*(7), 576-589.

Zhang, N., Arroyo, M., Ciantia, M.O., Gens, A., Butlanska, J., (2019). Standard penetration testing in a virtual calibration chamber. *Computers and Geotechnics* 111, 277–289.

Zhang, Z., & Wang, Y. H. (2015). Examining setup mechanisms of driven piles in sand using laboratory model pile tests. *J. Geotech. Geoenviron*, *141*(3), 04014114.